American Mineralogist, Volume 91, pages 1089–1093, 2006

$Ba(NpO_2)(PO_4)(H_2O)$, its relationship to the uranophane group, and implications for Np incorporation in uranyl minerals

TORI Z. FORBES AND PETER C. BURNS*

Department of Civil Engineering and Geological Sciences, University of Notre Dame, Notre Dame, Indiana 46556, U.S.A

ABSTRACT

Single crystals of $Ba(NpO_2)(PO_4)(H_2O)$ were obtained using hydrothermal synthesis techniques. The structure was determined using single-crystal X-ray diffraction data collected using Mo$K\alpha$ radiation and an APEX II CCD detector and was refined on the basis of F^2 for all unique data to R_1 = 2.41%. $Ba(NpO_2)(PO_4)(H_2O)$ crystallized in monoclinic space group $P2_1/n$ with a = 6.905(3), b = 7.108(3), c = 13.321(6) Å, β = 105.02°, and V = 631.4 Å^3. The structure contains chains of edge-sharing neptunyl pentagonal bipyramids that link through phosphate tetrahedra to form infinite sheets. This sheet-type is identical to the anion topology of the uranophane group, in particular to that of oursinite, $Co[(UO_2)(SiO_3OH)]_2(H_2O)_6$. Similarities between $Ba(NpO_2)(PO_4)(H_2O)$ and the uranophane group of minerals suggests a charge-balancing mechanism for incorporation of Np^{5+} into uranyl minerals.

Keywords: Neptunium, uranyl mineral, uranophane, nuclear waste, crystal structure, actinide

INTRODUCTION

A geologic repository for high-level nuclear waste, such as the proposed repository at Yucca Mountain, Nevada, is faced with the challenging task of controlling the fate of a chemically diverse suite of radionuclides, including ^{237}Np (Lieser and Muhlenweg 1988; Silva and Nitsche 1995). Commercial spent nuclear fuel is composed of 95–99% UO_2, with other actinides and fission products comprising the remainder (Johnson and Werme 1994). ^{237}Np, with a half-life of 2.14×10^6 years, is one of the key contributors to the total potential radiation dose after thousands of years for the proposed repository at Yucca Mountain. Due to the significance of ^{237}Np for the performance of a geologic repository, as well as its presence in sites contaminated by actinides, it is important to understand its fate and transport within natural systems (Kaszuba and Runde 1999; Lieser and Muhlenweg 1988; Silva and Nitsche 1995).

Laboratory studies and characterization of natural analogs indicate that commercial spent nuclear fuel is readily oxidized upon exposure to moist oxidizing conditions similar to those expected in the proposed repository at Yucca Mountain (Finch and Ewing 1992; Finch et al. 1999; Pearcy et al. 1994; Shoesmith 2000; Wronkiewicz et al. 1996). Interactions between spent fuel and groundwater of composition similar to that expected at Yucca Mountain results in extensive alteration of spent fuel, and formation of a variety of uranyl oxide hydrates and uranyl silicates (Finch et al. 1999; Finn et al. 1998). It is possible that such uranyl phases will significantly impact the mobility of uranium and any other radionuclide they incorporate.

Under oxidizing conditions, the dominate oxidation states of U and Np in solution are hexavalent and pentavalent, respectively (Antonio et al. 2001; Silva and Nitsche 1995). In both cases the cations are present in solutions and crystal structures as nearly linear dioxo cations, $(UO_2)^{2+}$ and $(NpO_2)^+$, with bond lengths ~1.8 Å (Burns et al. 1997b). The actinyl cations are further coordinated by four, five, or six equatorial ligands to create square, pentagonal, and hexagonal bipyramids (Burns et al. 1997a, 1997b).

The crystal structures of the uranyl phases that are expected to form when spent fuel is altered under moist oxidizing conditions are dominated by sheets of uranyl polyhedra and other polyhedra containing higher-valence cations. In particular, the uranyl silicates found in tests involving spent fuel and UO_2 under unsaturated conditions (Finch et al. 1999; Wronkiewicz et al. 1996) contain uranophane-type sheets of uranyl pentagonal bipyramids and silicate tetrahedra, with low-valence cations and H_2O groups located in the interlayer regions. On the basis of the geometric similarities of $(UO_2)^{2+}$ uranyl polyhedra and $(NpO_2)^+$ neptunyl polyhedra, Burns et al. (1997b) predicted that significant Np^{5+} could be incorporated into uranyl phases that form as spent fuel is altered, and suggested that such incorporation could impact the mobility of Np^{5+} in a geological repository. However, substitution of Np^{5+} for U^{6+} in a crystal structure requires a charge-balance mechanism that may involve another substitution at some other type of site in the crystal structure. More recently, incorporation of Np^{5+} into powders of synthetic uranophane and the Na analog of compreignacite has been demonstrated (Burns et al. 2004), although the charge-balance mechanism that permits incorporation is uncertain.

We are examining the crystal chemistry of Np^{5+} to better understand the fate of Np contamination in natural systems. This involves the synthesis and structural characterization of a variety of Np^{5+} compounds containing environmentally relevant cations and anions. Here we describe the synthesis and structure of a novel Np^{5+} phosphate that is structurally related

* E-mail: pburns@nd.edu

0003-004X/06/0007–1089$05.00/DOI: 10.2138/am.2006.2132

to the uranophane group of uranyl silicates, and discuss the possible role of phosphate in facilitating the substitution of Np^{5+} for U^{6+} in uranyl silicates.

Experimental methods

Single crystals of $Ba(NpO_2)(PO_4)(H_2O)$ were grown hydrothermally using 125 mL Teflon-lined Parr acid reaction vessels. A 0.107 *M* Np^{5+} stock solution was prepared in a 1 *M* HCl solution. Note: All syntheses were completed at Argonne National Laboratory in facilities capable of handling radioactive material. Fluoroapatite from the Liscombe deposit near Wilberforce, Ontario, Canada was used as the source of phosphate. $Ba(NpO_2)(PO_4)(H_2O)$ was synthesized by the hydrothermal reaction of 0.0256 g $Ca_5(PO_4)_3F$ and 0.2513 g of $BaCl_2$ (Fisher Scientific Lot no. 724112) with 0.23 mL of a 0.107 *M* Np^{5+} solution (5.9 mg Np) and 0.77 mL of ultra pure water (the final concentration of Np in the solution was 0.025 M). The initial pH of the solution was 0.10. The reactants were placed in a 7 mL Teflon cup fitted with a screw-top lid. The Teflon cup was then tightly capped and placed into the 125 mL Teflon-lined Parr acid reaction vessel. Fifty milliliters of ultrapure water (18 MΩ resistance) was added to the vessel to provide counter-pressure during heating. The reactants were heated for one week at 150 °C in a gravity convection oven, and were allowed to cool slowly in the oven. Sprays of dark green needles approximately 600 μm in length formed during the reaction.

A single crystal with dimensions of 300 × 50 × 10 μm was mounted on a glass fiber and placed on a Bruker PLATFORM three-circle X-ray diffractometer equipped with an APEX II CCD detector. A sphere of three-dimensional data was collected at room temperature using monochromatic Mo*K*α X-radiation, frame widths of 0.3° in ω, and 10 s spent counting per frame. The unit-cell parameters were refined by least-squares techniques using the Bruker APEX II software. Selected data collection parameters and crystallographic data are provided in Table 1.

The intensity data were reduced and corrected for Lorentz, polarization and background effects using the Bruker APEX II software. A semi-empirical absorption correction was applied using the Bruker program XPREP by modeling the crystal as a plate, which lowered the R_{int} from 0.0706 to 0.0595. $Ba(NpO_2)(PO_4)(H_2O)$ crystallizes in the monoclinic space group $P2_1/n$. The structure was solved by direct methods and refined on the basis of F^2 for all unique reflections using the Bruker SHELXTL Version 5 system of programs. Atomic scattering factors for each atom were taken from *International Tables for X-ray Crystallography* (Ibers and Hamilton 1974). The Np and Ba atoms were located in a direct-method solution and the P and O atoms were located in difference-Fourier maps calculated following refinement of the partial-structure models. Possible H atom positions consistent with expected configurations were located in the difference-Fourier maps, and H positions were refined using the soft constraint that O-H bonds be ~0.96 Å. The final structural model included anisotropic displacement parameters for all atoms except H, and the refinement converged to an R_1 value of 0.024 for 1727 unique reflections ($F_o \geq 4\sigma$), and 0.035 for all 2356 reflections. The atomic positional parameters and anisotropic displacement parameters are given in Table 2 and selected interatomic distances and angles are given in Table 3.

Structure description

The structure of $Ba(NpO_2)(PO_4)(H_2O)$ is composed of chains of neptunyl polyhedra that are linked through phosphate tetrahedra to form infinite sheets. The structure contains one symmetrically independent Np^{5+} cation that is strongly bonded to two O atoms. This creates a nearly linear NpO_2^+ cation with bond lengths of 1.850(4) and 1.855(4) Å, which is consistent with the pentavalent state of Np. The NpO_2^+ cation is further coordinated in the equatorial plane by five O atoms that are located at the vertices of pentagonal bipyramids that are capped by the neptunyl ion O atoms. The bond lengths for the Np^{5+}-O_{eq} interactions range from 2.362(3) to 2.576(3) Å. One symmetrically distinct phosphate tetrahedron is present in the structure, with P-O bond lengths ranging from 1.504(4) to 1.583(3) Å.

The neptunyl pentagonal bipyramid shares its equatorial O1-O2 edge with a neighboring and symmetrically identical bipyramid, creating a chain of neptunyl polyhedra. Phosphate tetrahedra are attached to each side of the chain by sharing an edge with the neptunyl polyhedra. A single O5 vertex is shared between the phosphate tetrahedron of one chain and a neptunyl pentagonal bipyramid of an adjacent chain, resulting in an infinite two-dimensional neptunyl phosphate sheet (Fig. 1a).

The neptunyl phosphate sheets are linked through bonding to interstitial Ba^{2+} cations and by H bonding involving H_2O groups (Fig. 1b). One symmetrically independent Ba^{2+} cation is present, which is coordinated by ten O atoms with interatomic distances ranging from 2.730(3) to 3.281(3) Å. One H_2O group (O7) is located in the interlayer and forms H bonds with O atoms of the sheet. The H bonds extend from O7 to the O acceptors of the phosphate tetrahedra [O3 and O5, respectively]. The O acceptor lengths are 2.65 Å for H1-O3 and 2.54 Å for H2-O5.

Table 1. Unit-cell parameters, crystallographic parameters, and data statistics for $Ba(NpO_2)(PO_4)(H_2O)$

a (Å)	6.905(3)	Crystal size (μm)	300 × 50 × 10
b (Å)	7.108(3)	Radiation	Mo*K*α
c (Å)	13.321(6)	Data Range (θ)	3.17–33.56
β (°)	105.02	Total ref.	9634
V (Å^3)	631.4	Unique ref.	2356
Space group	$P2_1/n$	Largest diff. Peak and hole (Å^{-3})	1.797 and –2.441
F(000)	888	Final R_1 (%)	2.41
μ (mm^{-1})	22.798	Final wR_2 (%)	4.07
D_{calc} (g/cm^3)	5.463	S	0.798
Frame width	0.3° (ω)		
Frame time	10 s		
Unit-cell contents 4 $Ba(NpO_2)(PO_4)(H_2O)$			

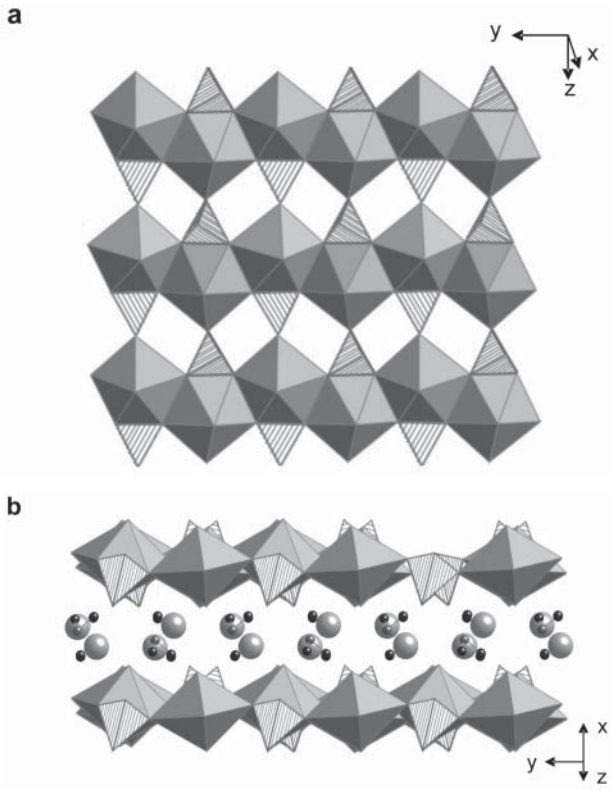

Figure 1. The structure of $Ba(NpO_2)(PO_4)(H_2O)$ contains (**a**) sheets of neptunyl pentagonal bipyramids and phosphate tetrahedra linked through (**b**) Ba atoms and water groups located in the interlayer.

Discussion

Over 200 of the 355 structures reported for uranyl minerals and other inorganic uranyl compounds contain infinite sheets of polyhedra of higher bond-valence (Burns 2005). The dominance of sheets of polyhedra in uranyl compounds is due to the unequal distribution of bond strengths within the uranyl polyhedron (Burns et al. 1997a). The O atoms of the uranyl ion are nearly satisfied by bonding to the U^{6+} cation alone, and as such do not generally bond to other higher valence cations. The equatorial ligands of the bipyramids are not satisfied by the bond to the U^{6+} cation alone and participate in additional bonding to neighboring polyhedra, thus favoring the formation of sheets (Burns 2005).

Burns et al. (1996) and Burns (1999) developed a hierarchy of structures of uranyl compounds, and in the case of sheets of polyhedra, the structures were arranged on the basis of the topological arrangement of the anions within the sheets. Projection of their topological information on a plane results in the sheet anion topology, which is a two-dimensional tiling of space with various polygons. The neptunyl phosphate sheet in $Ba(NpO_2)(PO_4)(H_2O)$ corresponds to the sheet anion-topology shown in Figure 2a, which was earlier designated as the uranophane sheet-anion topology by Burns et al. (1996). The structures of 17 uranyl compounds are based upon this topology, and 11 of these are minerals. $Cs(NpO_2)(CrO_4)(H_2O)$ is the only other Np^{5+} structure known that contains sheets based upon the uranophane anion topology (Grigor'ev et al. 1991).

The structure of $Ba(NpO_2)(PO_4)(H_2O)$ is closely related to those of the uranophane group of uranyl silicate minerals. These minerals contain sheets based upon the uranophane anion-topology in which the triangles of the anion topology correspond to the faces of silicate tetrahedra (Burns 2005). There are three known graphical isomers of the uranyl silicate sheet that differ in the orientation of the silicate tetrahedra. The uranophane sheet anion-topology contains mutually perpendicular chains of two types: those composed of edge-sharing squares and triangles (designated S-T) and those composed of pentagons and triangles that share edges and vertices (P-T). The latter of these was designated a **U** arrowhead chain by Miller et al. (1996). Different isomers of the uranophane sheet are distinguished by the orientation of the silicate tetrahedra along the (S-T) chains. In the case of the α-uranophane-type sheet, the silicate tetrahedra along the S-T chain alternate up (U) and down (D) with the sequence UDUDUD… and the tetrahedra contained in the P-T chains either point all up or all down (Fig. 2b) (Burns 1999). In β-uranophane the silicate tetrahedra along the S-T chains are oriented UUDDUUDD…, and along the P-T chains the tetrahedra point all up or all down (Fig. 2c) (Burns 1999). In oursinite, $(Co[(UO_2)(SiO_3OH)]_2(H_2O)_6)$ (Kubatko and Burns 2005), the tetrahedra in both the S-T and P-T chains alternate UDUDUD… (Fig. 2d). The sheet in $Ba(NpO_2)(PO_4)(H_2O)$ is topologically identical to that found in oursinite.

The uranophane group of minerals is the most abundant of the uranyl minerals. They occur as alteration products of uraninite in the Nopal I deposits, which are a natural analog for the proposed geological repository for nuclear waste at Yucca Mountain (Burns 1999; Pearcy et al. 1994). Uranophane-group minerals have also formed during the alteration of spent nuclear fuel and UO_2 in tests under hydrologically unsaturated conditions (Finch et al. 1999; Wronkiewicz et al. 1996). Substitution of Np^{5+} for U^{6+} in the structures of uranophane-group minerals could significantly impact the mobility of Np in a geological repository (Burns et al. 2004; Burns et al. 1997b), but a charge-balance mechanism must also occur.

Synthesis of $Ba(NpO_2)(PO_4)(H_2O)$ demonstrates that Np^{5+} is compatible with a sheet that is based upon the uranophane sheet anion-topology. Substitution of Np^{5+} for U^{6+} in the uranophane-type sheet requires that the structure is able to accommodate both the strain associated with incorporating the larger Np^{5+} cation, as compared with U^{6+}, and the necessary charge-balancing substitution elsewhere in the structure. The structure of $Ba(NpO_2)(PO_4)(H_2O)$ presents a scenario for satisfying each of these factors. The coupled substitution of $(NpO_2)^+ + (PO_4)^{3-}$ for $(UO_2)^{2+} + (SiO_4)^{4-}$ accounts for the necessary charge-balance. The typical U^{6+}-O equatorial bond-length for a pentagonal bipyramid is 2.37(10) Å (Burns 2005), whereas the corresponding Np^{5+}-O distance is about 0.1 Å longer (Burns et al. 1997b). The effective ionic radius of $^{[4]}P^{5+}$ is 0.09 Å shorter than that of $^{[4]}Si^{4+}$

Table 2. Atomic parameters and displacement parameters for $Ba(NpO_2)(PO_4)(H_2O)$

	x	*y*	*z*	U_{eq}		
Np1	0.7031(1)	0.7643(1)	0.1766(1)	0.010(1)		
Ba1	0.2154(1)	0.4401(1)	0.1433(1)	0.016(1)		
P1	0.8430(2)	0.7792(2)	0.4226(1)	0.011(1)		
O1	0.7188(5)	0.0999(4)	0.1451(2)	0.014(1)		
O2	0.6383(5)	0.4321(4)	0.1608(2)	0.013(1)		
O3	–0.1819(5)	0.3373(5)	0.0264(2)	0.016(1)		
O4	0.9487(5)	0.7123(4)	0.6973(2)	0.012(1)		
O5	0.5540(5)	0.7434(4)	–0.0039(2)	0.016(1)		
O6	0.9620(6)	0.7296(5)	0.1652(2)	0.019(1)		
O7	0.1597(8)	0.0614(6)	0.1251(4)	0.038(1)		
H1	0.232(10)	–0.043(9)	0.101(5)	0.050		
H2	0.184(11)	0.079(10)	0.070(5)	0.050		
	U_{11}	U_{22}	U_{33}	U_{23}	U_{13}	U_{12}
Np1	0.012(1)	0.008(1)	0.008(1)	–0.001(1)	0.001(1)	0.000(1)
Ba1	0.017(1)	0.013(1)	0.018(1)	0.002(1)	0.005(1)	0.000(1)
P1	0.015(1)	0.008(1)	0.008(1)	0.000(1)	0.001(1)	0.001(1)
O1	0.023(2)	0.008(2)	0.010(1)	0.005(1)	0.000(1)	0.002(1)
O2	0.025(2)	0.006(2)	0.006(1)	–0.002(1)	–0.001(1)	0.000(1)
O3	0.015(2)	0.020(2)	0.014(2)	0.002(1)	0.007(1)	0.001(2)
O4	0.016(2)	0.014(2)	0.006(2)	0.003(1)	0.003(1)	–0.001(1)
O5	0.017(2)	0.020(2)	0.008(1)	0.001(1)	0.001(1)	–0.002(2)
O6	0.017(2)	0.019(2)	0.025(2)	0.001(1)	0.013(2)	0.000(2)
O7	0.038(3)	0.021(2)	0.058(3)	0.003(2)	0.016(2)	0.004(2)

Table 3. Selected interatomic distances (Å) and angles (°) in $Ba(NpO_2)(PO_4)(H_2O)$

Np(1)-O6	1.850(4)	Ba1-O3[d]	2.720(3)
Np(1)-O4[a]	1.855(4)	Ba1-O7	2.721(5)
Np(1)-O5	2.362(3)	Ba1-O6[e]	2.765(4)
Np(1)-O2	2.403(3)	Ba1-O4[f]	2.865(3)
Np(1)-O1	2.429(3)	Ba1-O2	2.869(4)
Np(1)-O2[b]	2.467(3)	Ba1-O3	2.876(3)
Np(1)-O1[c]	2.576(3)		
O6-Np(1)-O4[a]	175.50(14)		
P1-O3[g]	1.504(4)		
P1-O5[h]	1.539(4)		
P1-O1[c]	1.555(3)		
P1-O2[b]	1.583(3)		

Notes: Symmetry transformations used to generate equivalent atoms: a = x – 7/2, –y + 5/2, z – 5/2; b = –x + 3/2, y + 1/2, –z + ½; c = –x + 3/2, y – 1/2, –z + ½; d = –x, –y+1, –z; e = x – 1, y, z; f = –x + 4, –y + 2, –z + 3; g = –x + 1/2, y + 1/2, –z + ½; h = x + 1/2, –y + 3/2, z + ½.

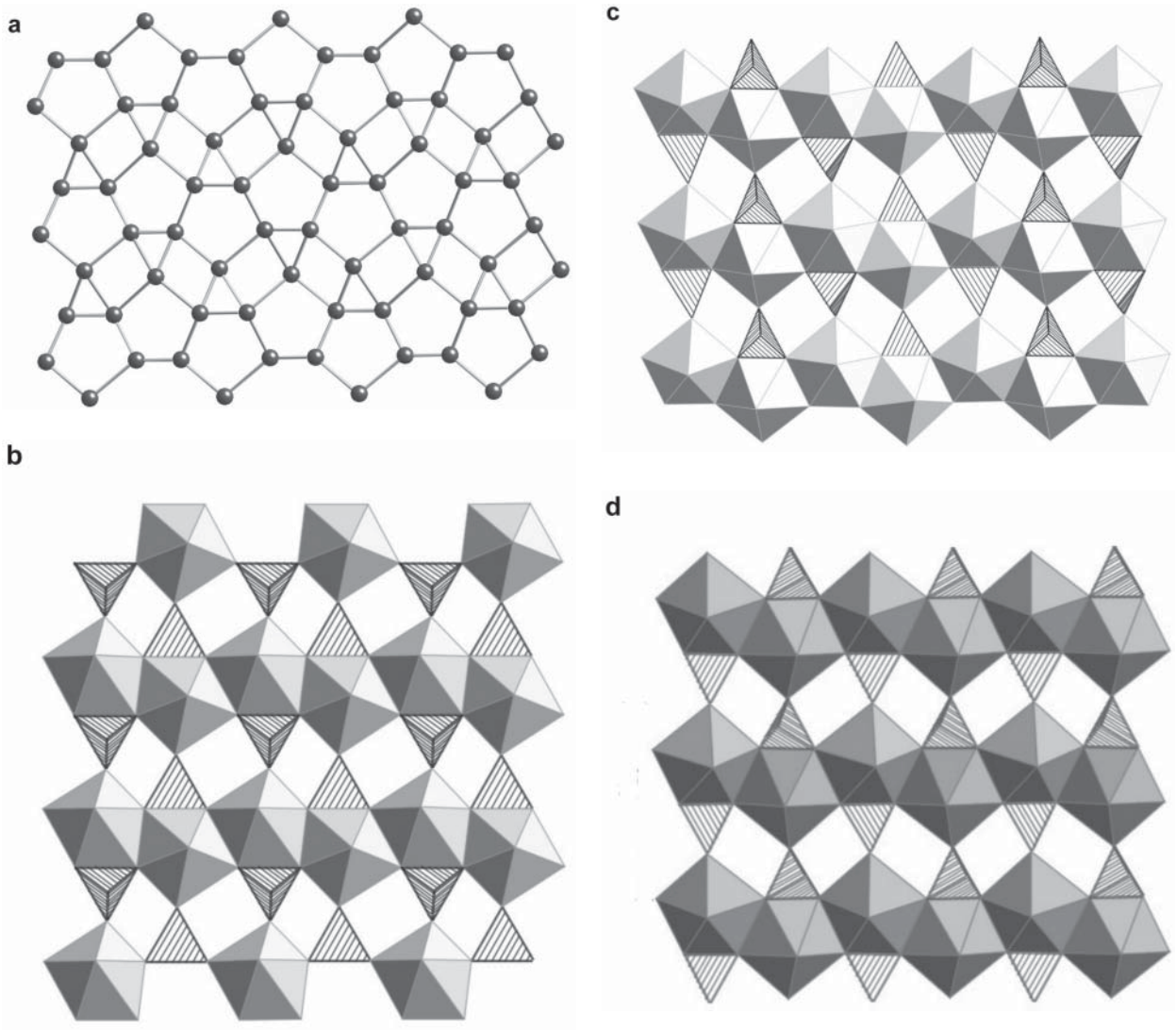

FIGURE 2. The uranophane sheet-type anion topology containing edge-sharing pentagons separated by chains of edge-sharing triangles and squares (**a**). Three graphical isomers exist for the uranyl silicate sheets of the uranophane group. These are distinguished by the direction the apical ligand on the tetrahedron extends. Sheets in the structures of (**b**) α-uranophane, (**c**) β-uranophane, and (**d**) oursinite and $Ba(NpO_2)(PO_4)(H_2O)$.

(Shannon 1976). Thus, should this coupled substitution occur on a local scale, such that an adjacent pentagonal bipyramid and tetrahedron are both involved, the strain associated with the substitution of the larger Np^{5+} cation for U^{6+} may be largely alleviated by substitution of a smaller phosphate tetrahedron in place of the silicate tetrahedron. As such, the presence of even small quantities of phosphate may provide for the incorporation of Np^{5+} into uranophane-group minerals, although experimental verification is needed. Substitution of phosphate for silicate in trace amounts in silicate minerals is well known (e.g., feldspars, Smith and Brown 1988), as is silicate substitution for phosphate in the apatite structure (Kim et al. 2003; Tang et al. 2005).

ACKNOWLEDGMENTS

This research was supported by the National Science Foundation Environmental Molecular Science Institute at the University of Notre Dame (EAR02-21966) and the Environmental Management Science Program of the Office of Science, U.S. Department of Energy, grants DE-FG07-97ER14820 and DE-FG03-97SF14749, as well as the Office of Civilian Radioactive Waste Management Science and Technology program. This report was prepared by University of Notre Dame pursuant to a cooperative agreement (DE-FC28-04RW12255) funded by the United States Department of Energy (DOE), Office of Civilian Radioactive Waste Management (OCRWM), Office of Science and Technology and International (OST&I), and neither, University of Notre Dame, nor any of its contractors or subcontractors, nor the DOE/OCRWM/OST&I, nor any person acting on behalf of either: Makes any warranty or representation, express or implied, with respect to the accuracy, completeness, or usefulness of the information contained in this report, or that the use of any information, apparatus, method, or process disclosed in this report may not infringe privately owned rights; or Assumes any liabilities with respect to the use

of, or for damages resulting from the use of, any information, apparatus, method, or process disclosed in this report. Reference herein to any specific commercial product, process, or service by trade name, trademark, manufacturer, or otherwise, does not necessarily constitute or imply its endorsement, recommendation, or favoring by DOE/OCRWM/OST&I. The views, opinions, findings, and conclusions or recommendations of authors expressed herein do not necessarily state or reflect those of the DOE/OCRWM/OST&I. We also thank Lynne Soderholm, S. Skanthakumar, Mark Sreniawski, and Ed Diaz for their help while conducting research at Argonne National Laboratory.

REFERENCES CITED

Antonio, M.R., Soderholm, L., Williams, C.C., Blaudeau, J.-P., and Bursten, B.E. (2001) Neptunium Redox Speciation. Radiochimica Acta, 89, 17–25.

Burns, P.C. (1999) The Crystal Chemistry of Uranium. In P.C. Burns and R. Finch, Eds., Uranium: Mineralogy, Geochemistry and the Environment, 38, 23–90. Reviews in Mineralogy, Mineralogical Society of America, Chantilly, Virginia.

——— (2005) U^{6+} Minerals and Inorganic Compounds: Insights into an Expanded Structural Hierarchy of Crystal Structures. Canadian Mineralogist, 43, 1839–1894.

Burns, P.C., Ewing, R.C., and Hawthorne, F.C. (1997a) The crystal chemistry of hexavalent uranium: polyhedron geometries, bond-valence parameters, and polymerization of polyhedra. Canadian Mineralogist, 35, 1551–1570.

Burns, P.C., Ewing, R.C., and Miller, M.L. (1997b) Incorporation mechanisms of actinide elements into the structures of U^{6+} phases formed during the oxidation of spent nuclear fuel. Journal of Nuclear materials, 245, 1–9.

Burns, P.C., Deely, K.M., and Skanthakumar, S. (2004) Neptunium incorporation into uranyl compounds that form as alteration products of spent nuclear fuel: Implications for geologic repository performance. Radiochimica Acta, 92, 151–159.

Finch, R.J. and Ewing, R.C. (1992) Corrosion of uraninite under oxidizing conditions. Journal of Nuclear Materials, 190, 133–156.

Finch, R.J., Buck, E.C., Finn, P.A., and Bates, J.K. (1999) Oxidative corrosion of spent UO_2 fuel in vapor and dripping groundwater at 90 °C. Materials Research Symposium Proceedings, 556, 431–438.

Finn, P.A., Finch, R., Buck, E., and Bates, J. (1998) Corrosion mechanisms of spent fuel under oxidizing conditions. Materials Research Society Symposium, 506, 123–131.

Grigor'ev, M.S., Baturin, N.A., Fedoseev, A.M., and Budantseva, N.A. (1991) Crystal and molecular structure of neptunium(V) complex chromates Cs $NpO_2(CrO_4)H_2O$ and $(NH_4)_4(NpO_2)_2(CrO_4)_3$. Radiokhimiya, 33(5), 53–63.

Ibers, J.A. and Hamilton, W.A. (1974) International Tables for X-ray Crystallography, IV. Kynoch Press, Birmingham, U.K.

Johnson, L.H. and Werme, L.O. (1994) Materials Characteristics and Dissolution Behavior of Spent Nuclear Fuel. MRS Bulletin(December), 24–27.

Kaszuba, J.P. and Runde, W.H. (1999) The Aqueous Geochemistry of Neptunium: Dynamic Control of Soluble Concentrations with Applications to Nuclear Waste Disposal. Environmental Science and Technology, 33, 4427–4433.

Kim, S.R., Lee, J.H., Kim, Y.T., Riu, D.H., Jung, S.J., Lee, Y.J., Chung, S.C., and Kim, Y.H. (2003) Synthesis of Si, Mg substituted hydroxyapatites and their sintering behaviors. Biomaterials, 24, 1389–1398.

Kubatko, K.-A. and Burns, P.C. (2006) A novel arrangement of silicate tetrahedra in the uranyl silicate sheet of oursinite, $(Co_{0.8}Mg_{0.2})[(UO_2)(SiO_3OH)]_2(H_2O)_6$. American Mineralogist, 91, 333–336.

Lieser, K.H. and Muhlenweg, U. (1988) Neptunium in the Hydrosphere and in the Geosphere. Radiochimica Acta, 43, 27–35.

Miller, M.L., Finch, R.J., Burns, P.C., and Ewing, R.C. (1996) Description and classification of uranium oxide hydrate sheet topologies. Journal of Materials Research, 11, 3048–3056.

Pearcy, E., Prikryl, J., Murphy, W., and Leslie, B. (1994) Alteration of uraninite from the Nopal I deposit, Pena Blanca District, Chihuahua, Mexico, compared to degradation of spent nuclear fuel in the proposed US high-level nuclear waste repository at Yucca Mountain, Nevada. Applied Geochemistry, 9, 713–732.

Shannon, R.D. (1976) Revised Effective Ionic Radii and Systematic Studies of Interatomic Distances in Halides and Chalcogenides. Acta Crystallographica, A32, 751–767.

Shoesmith, D.W. (2000) Review: Fuel corrosion processes under waste disposal conditions. Journal of Nuclear Materials, 282, 1–31.

Silva, R.J. and Nitsche, H. (1995) Actinide Environmental Chemistry. Radiochimica Acta, 70/71, 377–396.

Smith, J.V. and Brown, W.L. (1988) Feldspar Minerals 1. Crystal Structures, Physical, Chemical, and Microtextural Properties. Springer-Verlag, Berlin.

Tang, X.L., Xiao, F., and Liu, R.F. (2005) Structural characterization of silicon-substituted hydroxyapatite synthesized by a hydrothermal method. Materials Letters, 59, 3841–3846.

Wronkiewicz, D.J., Bates, J.K., Wolf, S.F., and Buck, E.C. (1996) Ten-year results from unsaturated drip tests with UO_2 at 90 °C: implications for the corrosion of spent nuclear fuel. Journal of Nuclear Materials, 238, 78–95.

MANUSCRIPT RECEIVED OCTOBER 27, 2005
MANUSCRIPT ACCEPTED MARCH 5, 2006
MANUSCRIPT HANDLED BY PRZEMYSLAW DERA